This is a repository copy of *High frequency inductor proximity loss calculation with 3D finite element analysis considering non-sinusoidal current distortion*.

White Rose Research Online URL for this paper:
https://eprints.whiterose.ac.uk/197800/

Version: Published Version

The 4th International Conference on Electrical Engineering and Green Energy CEEGE 2021, 10–13 June, Munich, Germany

High frequency inductor proximity loss calculation with 3D finite element analysis considering non-sinusoidal current distortion

Chaohui Liu[a],[*], Xiao Chen[b], Guidong Xiu[a], Liman Xiong[a], Lianghui Yang[a]

[a] *National New Energy Vehicle Technology Innovation Center, Beijing 100176, China*
[b] *University of Sheffield, Sheffield, S1 4WD, United Kingdom*

Abstract

This paper describes a 3D finite element (FE) based method to calculate the proximity losses for magnetic components in power conversion system. The proximity loss is the main concern of copper loss which causes ac losses in the winding. The FE model is built based on the definitions of the geometries, meshes, materials, electric circuits, boundary conditions, load conditions, as well as the characteristics of the wire. The total proximity loss is the sum of the power losses of each element calculated with the power loss density function using the obtained nodal flux densities via finite element analysis (FEA) at the given load condition. Owing to a detailed model with all the geometric parameters and thus the flux leakage and end-winding effects can be considered, this FEA approach can predict the flux density more accurately. In addition, non-sinusoidal current is analyzed to calculate the actual power loss in current distortion condition. Experimental tests have been implemented to validate the method. The approach is capable of calculating the energy consumption in power converter for efficiency approvement and energy management.

1. Introduction

Energy conversion with power converters is one of the key enabling techniques to convert the renewable energies, such as solar [1,2], hydro [3,4], and wind [5,6] energies, to electricity. To improve the power density of the power converters, the magnetic components, inductor and transformer, usually operate at high frequencies. However, this exacerbates the challenges in the energy management and efficiency estimation of power converters. Litz wires are widely used in these components to mitigate skin effect due to the fringing fields in the windings (coils) [7,8]. Litz

---

wire is usually constructed from small insulated strands, woven or twisted to distribute the current density over the entire cross-sectional area of the wire [9–11]. Thus, improvement of the power converter efficiency can be achieved as the skin effect can be reduced and homogeneous distribution of the conducted current is expected [7,12].

On the other hand, although the skin effect can be reduced owing to the twisted structure, the proximity loss is still considerable owing to the high external magnetic fields generated by adjacent strands [13–15]. Thus the accuracy of quantifying the achievable losses in a power converter is challenging since the ac resistance cannot be obtained directly but can only be estimated [16–21].

Since the proximity loss is caused by the external magnetic fields generated by adjacent strands if the magnetic field can be modeled with a reasonable accuracy, the proximity loss can be evaluated [22,23]. Several methods have been proposed to characterize the losses in magnetic components. In [9] a computational procedure was proposed to predict the losses in the realistic wire constructions by computing the equivalent ac resistance of a straight litz wire. However, the wire is only considered in the free air and the influence of the core winding effect in the actual inductor or transformer has not been considered. In [24], the squared-field-derivative method is proposed to calculate the proximity loss in round-wire. A frequency-independent matrix is derived to describe the transformer and inductor, by the use of a numerical magneto-static field calculation. However, it is still challenging to obtain the flux density since the geometries, structure and materials need to be taken into account. In addition, the analysis above mainly can be used in the applications where the current waveform is close to sinusoidal. Less study has been seen in the condition of large distortion where the current is non-sinusoidal.

This paper presents a 3D FEA method suitable for inductor proximity loss estimation in power converter. The FEA approach can predict the flux density in the core more accurately because FEA allows a detailed model with all the geometric parameters and thus the flux leakage effects can be considered; Therefore, the proximity loss can be predicted more accurately using FEA. This paper is organized as follows. Section 2 presents the 3D FEA method employed to characterize the inductor proximity loss. In Section 3, power loss is calculated based on the power density. Section 4 presents the results from which the methods have been verified with experimental measurements.

2. Proximity loss prediction approach

2.1. Proximity loss calculation procedure

The flow chart of the copper loss calculation with FEA is shown in Fig. 1. First, the 3D FE model is built with the definitions of its geometries, meshes, materials, mechanical motion, electric circuits, boundary conditions and load conditions. Subsequently, the flux density of each node in the core can be calculated via 3D FEA at the given load condition. Then, the flux density of each element is obtained using the nodal flux densities and the element-nodes relationships. Thereafter, calculate the weighted arithmetic mean of all the element flux density squares by weighting element volumes. After this, the winding proximity loss is calculated using the weighted arithmetic mean of all the element flux densities. Finally, the winding proximity loss can be obtained by summing the DC loss and AC loss which is the proximity loss because the skin effect is negligible.
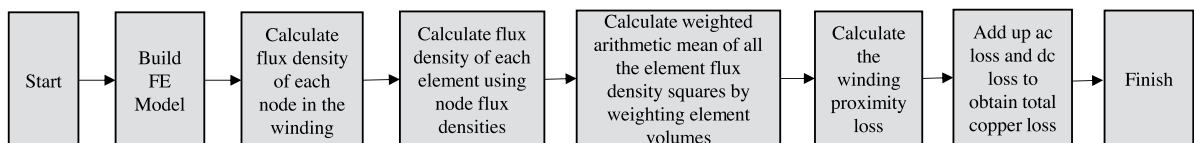
Fig. 1. Flow chart of the calculation procedure.

2.2. FE model

The FE tool FLUX 3D developed by Altair [25] is employed to build the 3D FE model of the inductor and subsequently perform the proximity loss calculation. Fig. 2. shows the inductor geometries built in the 3D FE model. It can be seen that the end-winding part is also modeled. The electric circuit model is shown in Fig. 3. and the winding current is determined by the current defined in the current source. The core material used in this
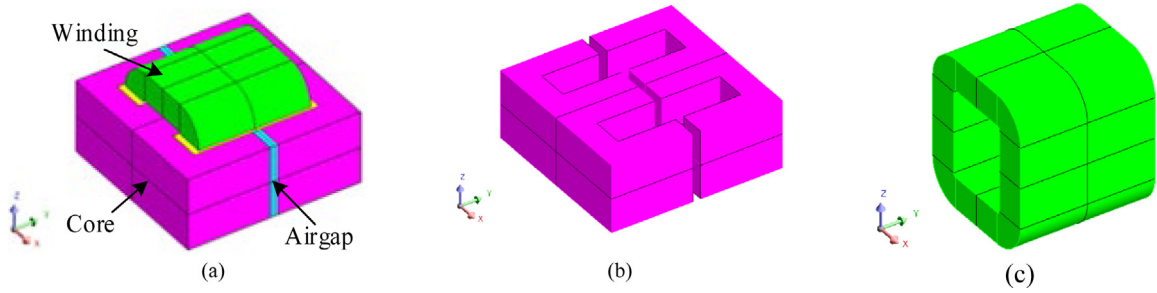
Fig. 2. Inductor geometries in the 3D FE model. (a) Winding and core. (b) Core. (c) Winding.
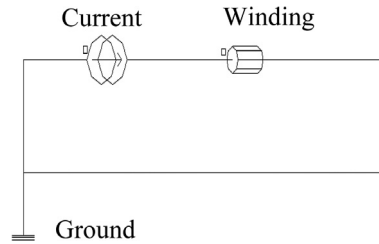
Fig. 3. Inductor electric circuit model.
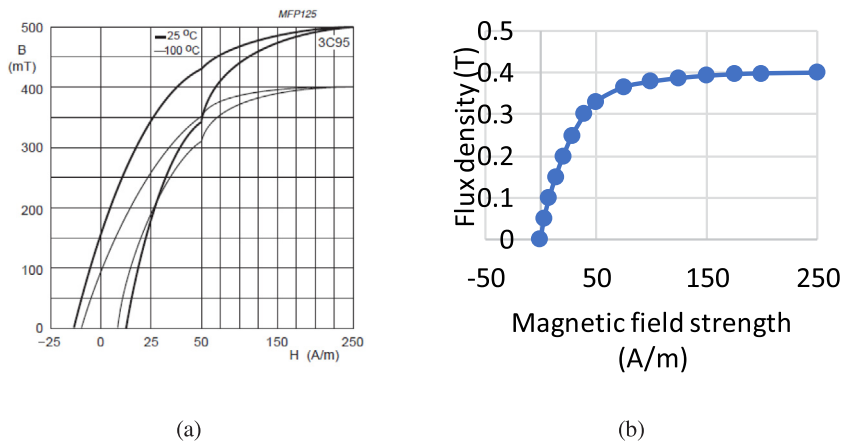
Fig. 4. B-H curve of the core material 3C95. (a) Datasheet. (b) Rebuild with uniform scale.

application is 3C95 whose datasheet B-H curve is illustrated in Fig. 4. (a). Its B-H curve with uniform scale at 100 °C is presented in Fig. 4. (b).

Given that the magnetic field in the full model satisfies the symmetry conditions along the *XOY*, *YOZ* and *ZOX* planes, the full model can be simplified and represented by one eighth of the model as illustrated in Fig. 5(a). The definitions of *XOY*, *YOZ* and *ZOX* planes can also be found in Fig. 5. The boundary conditions along *XOY* and *YOZ* planes are with tangent magnetic field and normal electric field while that along *ZOX* plane is with normal magnetic field and tangent electric field.
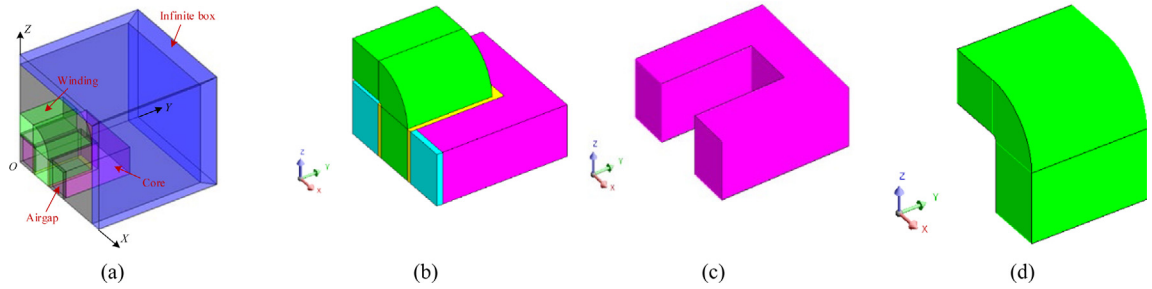
Fig. 5. Inductor 3D FE models (a) Full model. (b) Core, winding and airgap. (c) Core. (d) Winding.
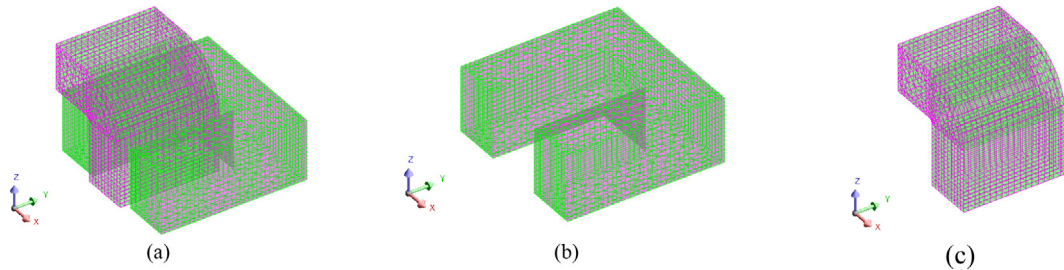
Fig. 6. 3D mesh of the inductor FE model. (a) Core and winding. (b) Core. (c) Winding.
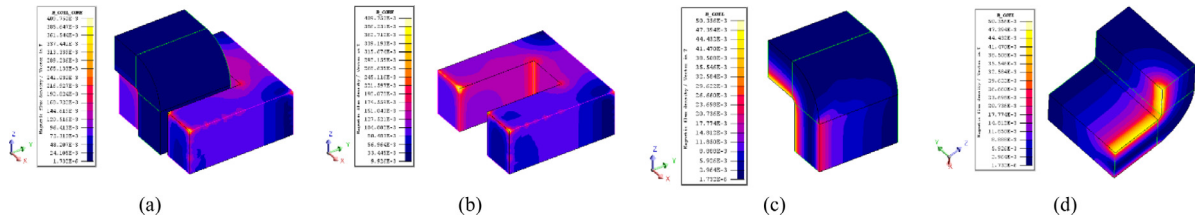
Fig. 7. Flux density contours of the inductor core and winding at 6A(RMS). (a) Core and winding. (b) Core. (c) Winding. (d) Winding.

Subsequently, the geometry built in Fig. 5 is meshed and Fig. 6 illustrates the mesh densities on the core and winding. It should be noted that the mesh in the 3D FE model cannot be as dense as that in the 2D model due to a much more computation needed in 3D FEA.

2.3. Nodal flux density

The FE model is run at 6 A RMS (assumed nominal current as sinusoidal waveforms for the sake of analysis) load condition with the static analysis. Subsequently, the resultant flux density contours of the inductor core and winding are illustrated in Fig. 7.

As can be seen, the flux densities over the inductor are non-uniform, particularly at its geometrical corners in which the localized effects are considerable. These localized effects cannot be captured by the conventional magnetic circuit-based method. In addition, from Fig. 7(c) and (d), it is clear that the flux densities at the winding corners close to the airgap, particularly the inner layer, are relatively higher than those in the other parts. This is because most of the flux leakage occurs in this area due to the presence of the airgap.

Subsequently, the flux density at each node of the winding is exported before the winding proximity loss calculation which will be discussed in next section.

Then, the flux density at each node is exported before the core loss calculation which will be discussed in the next section.

3. Proximity loss calculation

The proximity loss in the wire of the inductor can be calculated using (1) derived in Sullivan [24].

$$P_{px\_ind} = \frac{\pi L_t N_{ts} d_c^4}{64 \rho_c} \overline{\left\langle \left(\frac{dB_k}{dt} \right)^2 \right\rangle} \tag{1}$$

where P_{px_ind} is the inductor proximity loss, L_t represents the average length of one turn, N_{ts} is the product of the turn number per coil and the strand number per turn, d_c is the strand diameter, ρ_c is the wire resistivity, dB_k/dt is the time derivative of average flux density in kth element of the winding, $\langle \cdot \rangle$ is the spatial average operator and $\overline{(\cdot)}$ is the time average operator.

The current fed into the winding can be expressed as (2), neglecting the current harmonics.

$$i = I_m \sin (2\pi f t + \varphi) \tag{2}$$

where i is the winding transient current, I_m is the current amplitude, f represents the frequency, and φ represents the current initial phase angle.

Given that winding permeability is constant, the flux density B_k in the winding obtained at a given current with I_m amplitude can be calculated by linearly scaling the flux density B_{0k} at the reference current with I_{0m} amplitude, as described by (3). Therefore, only one 3D FEA with the reference current I_{0m} is needed to generate the nodal flux densities and thereafter the element flux densities.

$$B_k = \frac{I_m}{I_{0m}} B_{0k} \tag{3}$$

The flux density B_{0k} at the reference current with I_{0m} amplitude can be expressed as (4)

$$B_{0k} = B_{0km} \sin (2\pi f t + \varphi) \tag{4}$$

where B_{0km} is the average flux density amplitude in kth element at the reference current I_{0m}.

Based on (2), (3) and (4), the derivative of B_k against time is derived and shown in (5).

$$\frac{dB_k}{dt} = \frac{B_{0km}}{I_{0m}} \cdot \frac{di}{dt} \tag{5}$$

Substituting (5) into Eq. (1), the proximity loss in the inductor can be expressed as (6)

$$P_{px\_ind} = \frac{\pi L_t N_{ts} d_c^4}{64 \rho_c} \overline{\left\langle \left(\frac{dB_k}{dt} \right)^2 \right\rangle} \tag{6}$$

Therefore, the average flux density square over all the elements $\langle B_{0km}^2 \rangle$ at the reference current I_{0m} needs to be obtained. However, since the mesh sizes of the winding elements may be non-uniform, the average flux density square over all the elements $\langle B_{0km}^2 \rangle$ may not represent the true spatial average flux density square. Therefore, the weighted arithmetic mean of all the element flux density squares by weighting element volumes are employed to calculate the spatial average flux density square, as described in (7)

$$P_{px\_ind} = \frac{\pi L_t N_{ts} d_c^4}{64 \rho_c I_{0m}^2 V_{ol}} \langle B_{0km}^2 V_k \rangle \overline{\left(\frac{di}{dt} \right)^2} \tag{7}$$

where V_k is the volume of the kth element in the winding and V_{ol} is the total winding volume. The above equation implies that 3D computation of magnetic field and the resultant mean flux density over the winding volume only needs to be performed once with excitation of the reference current. Proximity loss at any current waveforms can be scaled accordingly as long as the conditions stated in [24] are satisfied.

The winding DC loss P_{DC} in the inductor can be calculated with the conventional equation shown in (8). where R_{DC} is the winding DC resistance which can be calculated with (9).

$$P_{DC} = \frac{1}{2} I_m^2 R_{DC} \tag{8}$$

$$R_{DC} = \frac{4\rho_c L_t N_{ts}}{\pi d_c^2} \tag{9}$$

Thus, the inductor copper loss is obtained by summing the proximity loss P_{px_ind} and the DC loss P_{DC}.

4. Experimental validation

To validate the calculation method, experimental tests are performed in the test rig. And the series inductor current and voltage are obtained with a YOKOGAWA oscilloscope.

4.1. Resistance measurement

The HIOKO LCR meter is used to measure the R_s and R_{dc} of the inductor coil. When the inductor has the core on, the measured R_s is 138.79 mΩ. In contrast, when the core is removed, only the coil is wound around the bobbin, and then the measured R_s is 69.20 mΩ. By changing the core area to air, the FE model can be employed to estimate the proximity loss in the coil without the influence of the core and then the corresponding ac resistance. In this case, the resultant ac resistance at 6.50 A is 71.09 mΩ and agrees well with the measured value of 69.20 mΩ in the air-cored inductor. From the resultant ac resistance above, it is clearly that the FE model has good accuracy with the measured resistance.

4.2. Power converter verification

To further verify the FE method for ac loss prediction, experimental tests have been implemented in a power converter. In the experimental DC–DC resonant power converter, the input DC link voltage is 383.70 V, the output side nominal battery voltage is 238.33 V, the nominal output current is 9.00 A. With the measurement of the inductor voltage and current, the actual losses in the inductor can be calculated and compared with the FEA result in the same condition. The measured voltage and current of the series inductor are obtained from the waveform data from the oscilloscope and plotted in Fig. 8 .

As can be see, inductor current waveform is close to sinusoidal, despite of a small distortion in the period immediate after the zero-crossing. The instantaneous power loss at each sampling time is calculated with the instantaneous voltage and current, and then the averaged power loss in one switching cycle is calculated. In this condition, the entire power losses of the inductor is 10.02 W, including 2.40 W core loss and 7.63 W copper loss.
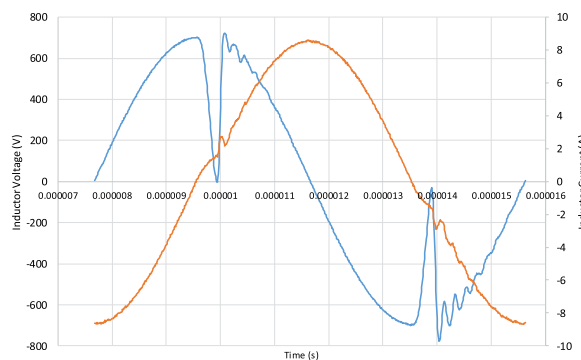
Fig. 8. Measured inductor voltage (in blue) and current (in red) waveforms.

The conventional prediction method described in Inoue and Akagi [26],Krismer and Kolar [27] is also applied to calculate the power loss. The measured R_s (no core in the inductor but only the coil winding in the bobbin) is 60 mΩ, the copper loss is 2.17 W, core loss is 2.60 W and the total loss is 4.77 W. The comparison of the three methods is shown in Table 1.

As can be observed from Table 1, the resultant copper loss from FEA model is 7.54 W, 1.18% less than the test results. However, the loss predicted by the conventional method is 2.17 W with 71.9% less than the measured results. The large error can be explained by the inaccuracy of the component datasheet, such as the ac resistance

Table 1. Summary Comparison of different methods.

Method	Measured (W)	FEA (W)	Conventional (W)
Total loss	10.02	9.92	4.77
Core loss	2.40	2.40	2.60
Copper loss	7.63	7.54	2.17
Error percentage	N/A	1.18%	71.9%

from the curve fitting, due to the lack of values in different temperatures. Overall, the FEA is clearly more accurate than the conventional prediction methodology, despite of the inaccuracy caused by the phase delay between the inductor voltage and current.

4.3. Non-sinusoidal current in high current distortion

The analysis above can be used in the applications where the current waveform is close to sinusoidal. However, when large distortion occurs in the current, the current used in the FEA method is not the RMS of the current anymore. Thus FFT needs to be applied and all the current distortions at each frequency are used to calculate the power loss with the magnetic field and then add up to get the total power loss.

In the experimental test system, the measurement in higher power is run at 3.5 kW power rating at 95.69 kHz. In this case, the battery voltage is 351.791 V, the DC link voltage is 387.835 V, and the discharging current is 8.984 A. The current in the inductor, ILs RMS, is 7.443 A. With the measured voltage and current from the experimental inductor, the actual power loss in the inductor can be calculated and compared with the FEA result in the same condition. The measured voltage and current of the series inductor is obtained from the waveform data from the oscilloscope and plotted in Fig. 9(a).
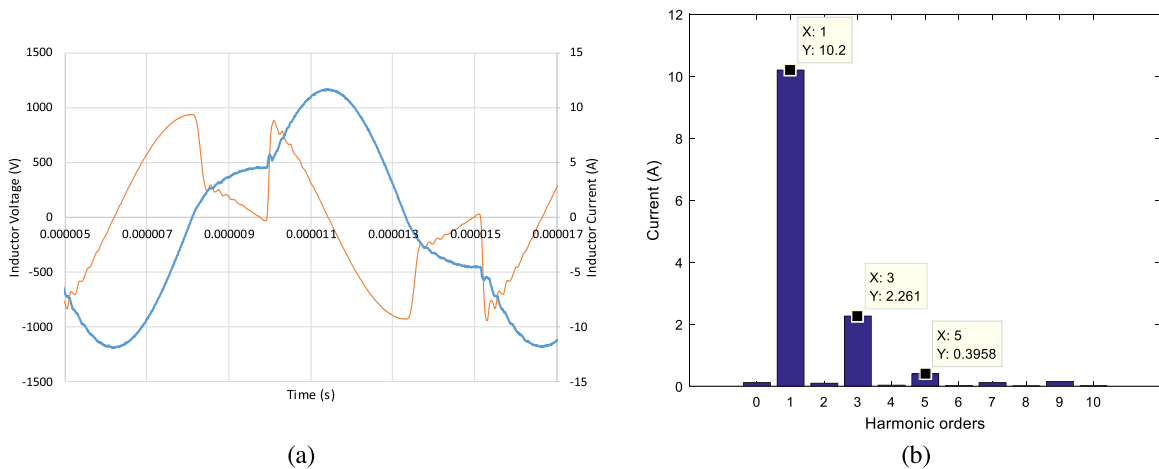

(a)   (b)

Fig. 9. Measured waveforms at 3.5 kW. (a) inductor voltage (in red) and current (in blue); (b) Harmonics of the current with current distortion.

As can be seen, the current of inductor is lagging the voltage, with a large distortion with flat area during DCM. The sampling rate of the oscilloscope is 100MS/s (corresponding resolution 1E-8). The switching frequency is 95.69 kHz, and thus 1045 sample points are recorded in one switching cycle. The instantaneous power loss at each sampling time is calculated with the instantaneous voltage and current, and then the averaged power loss in one switching cycle is calculated. In this condition, the total power loss is 26.06 W.

Then, the FEA method is also applied with the same condition. First the FFT analysis is carried out to find out the harmonic current values, as shown in Fig. 9. (b). The resultant copper loss, including DC copper loss, is 19.21 W. With core loss 6.22 W, the total loss in the inductor is 25.44 W. The conventional prediction method is also applied to calculate the power loss, and the total loss in the prediction is 11.22 W. The comparison is listed in Table 2.

Table 2. Comparison of three methods.

Method	Measured (W)	FEA (W)	Conventional (W)
Total loss	26.06	25.44	11.22
Core loss	6.22	6.22	6.22
Copper loss	19.83	19.21	4.99
Error percentage	N/A	2.30%	56.95%

As can be observed, compared with the measured copper loss 26.06 W, the resultant power loss from FEA model is 25.44 W, 2.30% less than the test results. This error may be caused by the inaccuracy in the phase measurement of the inductor voltage and current. However, despite of the inaccuracy in the phase measurement, the FEA method is clearly more accurate than the conventional method which is 11.22 W with 56.95% less than the test results.

5. Conclusion

In this paper, a 3D finite element (FE) method is presented to calculate the proximity losses for magnetic components in power conversion system. The design process is summarized for general use. The FE model is built based on the definitions of the geometries, meshes, materials, mechanical motion, electric circuits, boundary conditions and load conditions. The total proximity loss is the sum of the power losses of each element calculated with the power loss density function using the obtained nodal flux densities via finite element analysis (FEA) at the given load condition. In addition, this method also shows high accuracy with non-sinusoidal current when large distortion occurs in resonant converter. Measured results and experimental tests in a resonant power conversion system have validated that the calculation method is more accurate than conventional methods, and it is a suitable candidate for power loss analysis in power conversion systems. Future work will be focused on the transformer power loss estimation approach in power converter which enables the energy management for power converter.

Declaration of competing interest

The authors declare that they have no known competing financial interests or personal relationships that could have appeared to influence the work reported in this paper.

Acknowledgments

References

[1] Rahman E, Nojeh A. Harvesting solar thermal energy with a micro-gap thermionic-thermoelectric hybrid energy converter: Model development, energy exchange analysis, and performance optimization. Energy 2020;204:117947.

[2] Jeyasudha S, Geethalakshmi B. Modeling and performance analysis of a novel switched capacitor boost derived hybrid converter for solar photovoltaic applications. Sol Energy 2021;220:680–94.

[3] Zhang W, Dai L, Xiang Z, Wu Q, Huang S, Gao J. Optimal design of hydro permanent magnet synchronous generators for improving annual cycle efficiency. Int J Electr Power Energy Syst 2021;131:107096.

[4] Vasudevan KR, Ramachandaramurthy VK, Venugopal G, Ekanayake JB, Tiong SK. Variable speed pumped hydro storage: A review of converters, controls and energy management strategies. Renew Sustain Energy Rev 2021;135:110156.

[5] Hai Nguyen T, Thinh Quach N. A hybrid HVDC converter based on m2c and diode rectifiers without DC capacitors for offshore wind farm integration. Int J Electr Power Energy Syst 2021;133:107260.

[6] Hu C, Tong Y, Jing J, Zhao C. Research on steady state control strategies of wind farm integration by VSC-LCC hybrid HVDC transmission. Energy Rep 2020;6:985–91.

[7] Stadler A, Huber R, Stolzke T, Gulden C. Analytical calculation of copper losses in Litz-wire windings of gapped inductors. IEEE Trans Magn 2014;50(2):81–4.

[8] Etemadrezaei M, Lukic SM. Coated-strand Litz wire for multi-megahertz frequency applications. IEEE Trans Magn 2016;52(8):1–11.

[9] Zhang RY, White JK, Kassakian JG, Sullivan CR. Realistic Litz wire characterization using fast numerical simulations. In: 2014 IEEE applied power electronics conference and exposition. 2014. p. 738–745.

[10] Ferraro LD, Capponi FG. Aluminium multi-wire for high-frequency electric machines. In: 2007 IEEE industry applications annual meeting. 2007. p. 89–93.

[11] Mori K, Yamaguchi S, Higasiura A, Higuchi K. Development of parallel array multiple wire strip. In: Proceedings: Electrical electronics insulation conference and electrical manufacturing & coil winding conference. 1995. p. 247–51.

[12] v. d. Geest M, Polinder H, Ferreira JA, Zeilstra D. Stator winding proximity loss reduction techniques in high speed electrical machines. In: 2013 International electric machines & drives conference. 2013. p. 340–46.

[13] Chang RC, Chen CK, Wang CY, Tzou YY. Calculation of losses and temperature rise for high frequency transformer under forced-air convection. In: 36th Annual conference on IEEE industrial electronics society. 2010. p. 1–6.

[14] Eit MA, Bouillault F, Marchand C, Krebs G. 2-D reduced model for Eddy currents calculation in Litz wire and its application for switched reluctance machine. IEEE Trans Magn 2016;52(3):1–4.

[15] Petrov I, Polikarpova M, Ponomarev P, Lindh P, Pyrh?nen J. Investigation of additional AC losses in tooth-coil winding PMSM with high electrical frequency. In: 2016 XXII International conference on electrical machines. 2016. p. 1841–6.

[16] Qiong W, Xuning Z, Burgos R, Boroyevich D, White A, Kheraluwala M. Design considerations for a high efficiency 3 kW LLC resonant DC/DC transformer. In: In: Energy conversion congress and exposition. IEEE; 2015, p. 5454–61.

[17] Schmale I, Gleich B, Mende O, Borgert J. On the design of human-size MPI drive-field generators using RF Litz wires. In: 2015 5th International workshop on magnetic particle imaging. 2015. p. 1.

[18] Sibue JR, Meunier G, Ferrieux JP, Roudet J, Periot R. Modeling and computation of losses in conductors and magnetic cores of a large air gap transformer dedicated to contactless energy transfer. IEEE Trans Magn 2013;49(1):586–90.

[19] Stadler A. The optimization of high frequency inductors with litz-wire windings. In: 2013 International conference-workshop compatibility and power electronics. 2013. p. 209–13.

[20] Stadler A, Gulden C. Copper losses of Litz-wire windings due to an air gap. In: 2013 15th European conference on power electronics and applications. 2013. p. 1–7.

[21] Wang S, Dorrell DG. Copper loss analysis of EV charging coupler. IEEE Trans Magn 2015;51(11):1–4.

[22] Liu Z, Zhu J, Zhu L. Accurate calculation of Eddy current loss in litz-wired high-frequency transformer windings. IEEE Trans Magn 2018;54(11):1–5.

[23] Ehrlich S, Rossmanith H, Sauer M, Joffe C, März M. Fast numerical power loss calculation for high-frequency Litz wires. IEEE Trans Power Electron 2021;36(2):2018–32.

[24] Sullivan CR. Computationally efficient winding loss calculation with multiple windings, arbitrary waveforms, and two-dimensional or three-dimensional field geometry. IEEE Trans Power Electron 2001;16(1):142–50.

[25] CEDRAT. Flux V11.1.2 User Manual. Cedrat Company. accessed http://www.cedrat.com/en/software/flux.html.

[26] Inoue S, Akagi H. A bidirectional DC–DC converter for an energy storage system with galvanic isolation. IEEE Trans Power Electron 2007;22(6):2299–306.

[27] Krismer F, Kolar JW. Accurate power loss model derivation of a high-current dual active bridge converter for an automotive application. IEEE Trans Ind Electron 2010;57(3):881–91.